Unobtrusive Long-Range Detection of Passive RFID Tag Motion

Bing Jiang, *Student Member, IEEE*, Kenneth P. Fishkin, Sumit Roy, *Member, IEEE*, and Matthai Philipose

***Abstract*—This paper presents a novel method for detecting the motion of passive radio-frequency-identification (RFID) tags within the field of a detecting antenna. The method allows the unobtrusive detection of human interactions with RFID-tagged objects without requiring any modifications to existing communications protocols or RFID hardware. We use the response rate (a metric in lieu of the true received RF-signal intensity) at the reader to study the impact of tag translation, rotation, and coupling, as well as environmental effects. Performance is improved by introducing the idea of multiple tags/readers. Movement-detection algorithms are developed and integrated into the RFID monitoring system, and verified by experiments that demonstrate excellent results.**

***Index Terms*—Movement detection, passive tags, radio-frequency identification (RFID), radio-frequency (RF)-signal processing, response rate.**

I. Introduction

RADIO-FREQUENCY identification (RFID) is of growing interest due to recent declines in cost and size and increases in the working range. Current forecasts are for passive tags to be available for about $0.10 in a few years, with detection ranges in the few meters, and consequent annual deployments in the billions.

The RFID system consists of readers/interrogators and tags/transponders. RFID operates in different frequency bands (e.g., 125 kHz, 13.56 MHz, 868/915 MHz, 2.45 GHz, and 5.8 GHz). RFID has several important advantages over the traditional barcode.

1) It does not require line-of-sight (LoS) access to be read.
2) Multiple presenting tags can be read simultaneously.
3) Tags can be used in a rugged environment.
4) Tags can carry much more data.
5) Tags can be rewritable; they can modify their data as required.
6) Tags can be coupled with sensors to supply environmental information.

These features are enabling new RFID applications—e.g., to track objects in a supply chain, monitor their status, and enhance security [1].

Manuscript received April 30, 2004; revised October 3, 2005.

B. Jiang and S. Roy are with the Department of Electrical Engineering, University of Washington, Seattle, WA 98195 USA (e-mail: bjiang@u.washington.edu; roy@ee.washington.edu).

K. P. Fishkin and M. Philipose are with the Intel Research Seattle, Seattle, WA 98105 USA (e-mail: kenneth.p.fishkin@intel.com; matthai.philipose@intel.com).

Digital Object Identifier 10.1109/TIM.2005.861489

Tags may be categorized as either active or passive. The former have their own power supply, whereas the latter do not: tags are powered solely by radiated energy from an external source, such as an antenna on a tag reader. This absence of a power supply makes passive tags much cheaper and of much greater longevity than active tags, although their operating range, data-transfer rate, and computational abilities are much more limited. In this paper, we focus on passive tags, since these will almost certainly be deployed for the tracking of small individual objects.

An early forerunner of RFID technology was described in [2] that exploited the possibility of using reflected power to communicate. One of the earliest uses of RFID was in the identify: friend or foe (IFF) systems used to identify aircraft during World War II [3]. RFID became a commercial reality over the ensuing decades, with widespread deployment starting in the 1990s. Some important applications include toll collection, animal tracking, supply-chain management, and access control [3].

An important class of RFID applications within the ubiquitous computing framework consists of unobtrusively tracking the interactions of tagged objects with a human. For example, tagged medications could be monitored to avoid mismedication, tagged factory tools could be monitored to infer and monitor production methods, and tagged medical instruments could be monitored to prevent operating-room errors. However, current RFID systems typically provide only a binary output (presence/absence) for a particular tag.

In this paper, we use the RF-signal intensity that is backscattered to the reader from passive tags to characterize system response. Based on this method, algorithms for motion detection are developed and tested.

II. System-Modeling Principles

Interactions with RFID-tagged objects could be tracked in several ways.

A. Use Wearable/Handheld Readers

One solution is use small wearable readers, with short-range antennas in the palms [4]. When the user picks up an object, the wearable reader detects and transmits that event. A short operating range is preferred so that only the (single) tagged object grasped is read. While such readers can be made today, they require users to wear a special glove and reader apparatus, which may be unacceptable for many scenarios.

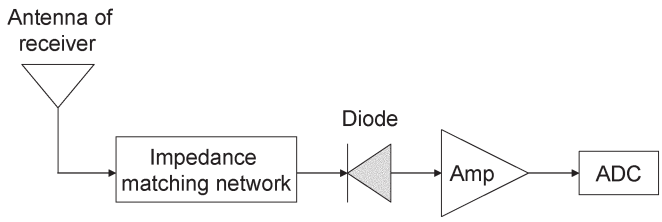

Fig. 1. RF-signal-intensity detector.

B. Use Acceleration-Detecting Tags

Object movement can be detected by measuring its acceleration. This implies that an accelerometer, an analog-to-digital converter, a digital controller, and a possible power source have to be integrated into the tag. The cost of such tags is too high to make them a feasible solution.

C. Detect Signal Intensity

RF-signal intensity decreases as a function of the distance between the transmitter to the receiver. Typically, it follows the inverse-square law for a free-space (ideal) environment, and with a higher path-loss exponent for indoor scenarios. When a tag is moved, the RF-signal intensity where the tag stays changes as well. Therefore, tag movement can be detected by measuring changes in the RF-signal intensity (Fig. 1) at either the reader or the tag. This approach could be pursued in several ways.

1) Intensity-Detecting Tags: It is easier to integrate an RF-signal intensity detector into a tag than an accelerometer, because only RF technology is used in the former, while both RF and microelectromechanical-system (MEMS) technologies are used in the latter. However, this approach would still increase cost, and require a new generation of RF tags.

2) Intensity-Detecting Readers: It is simpler, cheaper, and more feasible to modify readers rather than tags. However, there are a couple of problems.

1) Since the transmitter needs to keep emitting power continuously for the passive tags to respond, and the receiver generally includes an automatic-gain-control (AGC) loop, the accurate measurement of the RF signal at the reader is very difficult.
2) It is also difficult to identify the desired tag response (for measuring received-signal intensity) because multiple tags can respond simultaneously (i.e., the "tag collision problem"). Thus, appropriate signal-processing algorithms and protocols are required to disambiguate the desired tag response from the multiple returns.

While these obstacles could be overcome, they would again require new higher cost readers. We therefore investigate instead techniques that are effective with existing tags and readers without the need to modify either.

Instead of measuring the intensity at a signal tag directly, we infer it indirectly. Existing readers all support a "poll" command, wherein the reader transmits a batch command signal to all tags (i.e., N polls within a period of 1 s) and counts

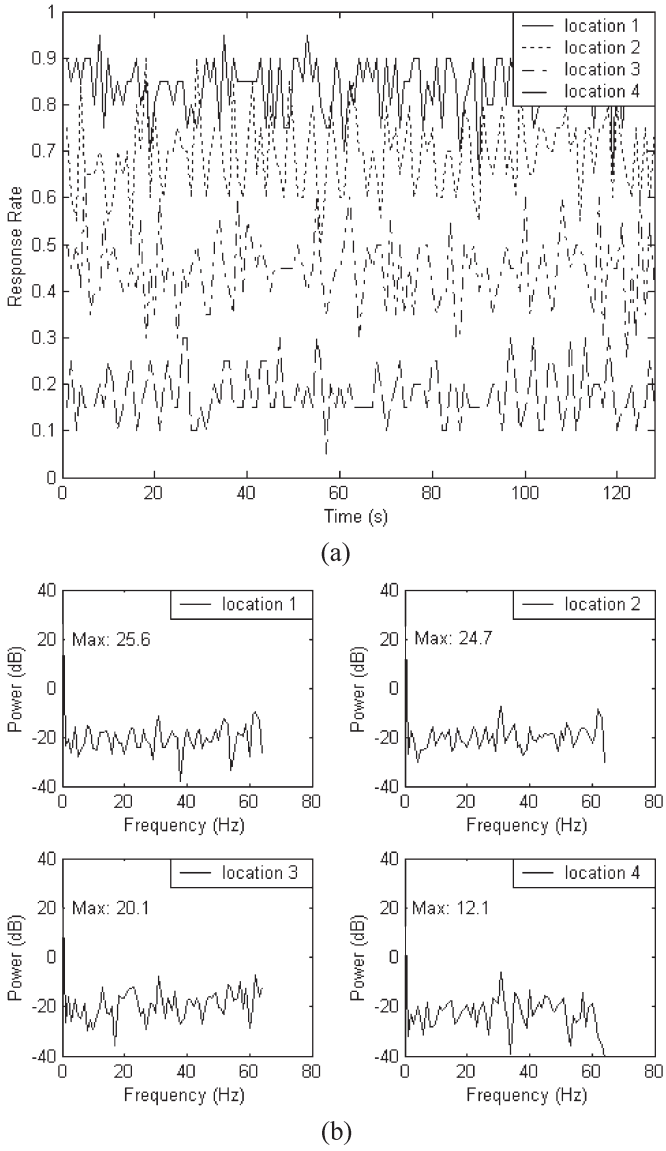

Fig. 2. Response rate at different locations, with $N = 20$ for a duration of 1 s. (a) Characteristics of response rate. (b) Power spectrum of response rate.

the number of responses received from that tag.[1] We therefore define a response rate α as

$$\alpha = \frac{N_{\mathrm{r}}}{N} \tag{1}$$

where N represents the number of polls and N_{r} is the count of responses to those polls. α is thus a dimensionless scalar between the values of 0 and 1. Fig. 2(a) shows the response rate of a tag at different locations in decreasing distance order from the reader, for a fixed orientation; Fig. 2(b) shows frequency-domain analysis based on the fast Fourier transform (FFT) of the observed raw α set at each location.

The results reveal the following:

1) The farther the tag, the lower the response rate in Fig. 2(a) as expected. This relationship is analogous to that of

[1]The backscatter from the passive tag to the reader uses a load resistor connected in parallel with the antenna that is switched on and off to modulate the data stream [5].

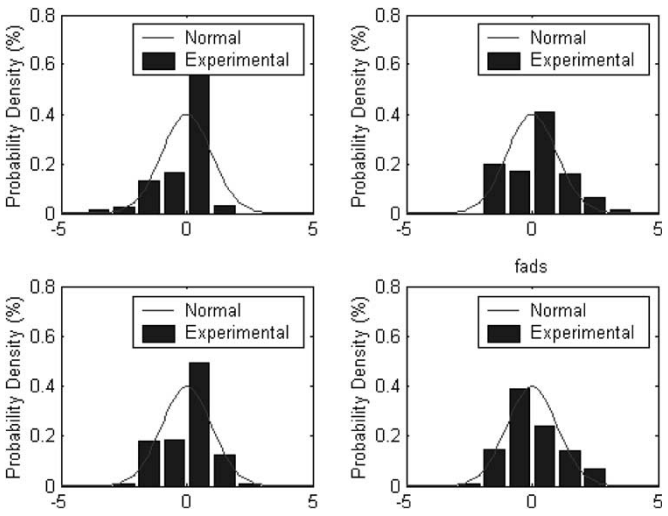

Fig. 3. Probability-density distribution of sample sets.

received RF-signal power with distance, and is the basis of our subsequent processing algorithm based on the response rate.

2) From the frequency analysis in Fig. 2(b), there are no significant periodic signal components in the response. The dc component of the response rate is proportional to the energy level and the variations about the mean may be considered as independent random perturbations. For a sample set $\Omega(\alpha_1, \alpha_2, \ldots, \alpha_{N_s})$, we introduce the following statistical parameters.

$$\alpha_{\text{mean}} = \frac{1}{N_s}\sum_{i=1}^{N_s}\alpha_i, \quad \alpha_{\text{rms}} = \sqrt{\frac{1}{N_s}\sum_{i=1}^{N_s}\alpha_i^2} \tag{2}$$

$$\sigma = \sqrt{\frac{1}{N_s - 1}\sum_{i=1}^{N_s}(\alpha_i - \alpha_{\text{mean}})^2} \tag{3}$$

$$\sigma_{\text{rel}} = \frac{\sigma}{\alpha_{\text{mean}}}, \quad \text{or} \quad \sigma'_{\text{rel}} = \frac{\sigma}{\alpha_{\text{rms}}} \tag{4}$$

where N_s is the size of Ω, and each element (α_i) of Ω corresponds to a set of N polls; α_{mean} is the mean of Ω; α_{rms} is the root mean square (rms) of Ω; σ is the standard deviation of Ω; σ_{rel} and σ'_{rel} are the relative standard deviations. Fig. 3 shows the probability-density function of the sample sets as shown in Fig. 2, where the x-axis is normalized by the standard deviation $(x = \alpha_i - \alpha_{\text{mean}}/\sigma)$. A key observation is that the normalized response rate is denser in the range $|x| \leq 1$ with a peak at zero, and there is almost no occurrence when $|x| \geq 3$. It follows that for sufficiently large N and N_s, the normalized response rate may be approximated by the standard normal-distribution model.

III. Characterization of the Response Rate

From elementary wave-propagation theory [6], it follows that

$$P_r = kP_t \tag{5}$$

where P_r is the received power after one-way propagation corresponding to a transmitted power of P_t and k is a scalar factor that is determined by the wavelength, distance, posture, and transmitting/receiving patterns. When the distance is large compared to the wavelength and the dimensions of the antennas, (5) can be written as the Friis transmission formula

$$P_r = \frac{A_{et}A_{er}}{d^2\lambda^2}P_t \tag{6}$$

where A_{et} is the effective aperture of the transmitting antenna; A_{er} is the effective aperture of the receiving antenna; d is the distance between the two antennas; λ is the wavelength. Since the impedance of the antenna is assumed to be matched, the received power is equal to the reradiated power on the same antenna [6]; therefore, the power P_{tr} that is reflected by a tag and received by the reader has the following relationship with the transmitted power

$$P_{tr} = P_r k = P_t k^2. \tag{7}$$

It is known that P_t is typically of the order of 30 dBm, and the superhet receiver that is usually employed in the readers offers a typical sensitivity greater than -150 dBm [7]. It can be derived from (5) and (7) that the minimum P_r at the tag that guarantees communication is of the order of -60 dBm, based on the detector requirements of a superhet-type reader. Note however that the tag IC will not respond until it receives enough power from the reader, and the reported minimum P_r required is of the order of -20 dBm [8], which exceeds -60 dBm. Therefore, the reader sees a detectable tag-response signal as long as the interrogating power at the tag exceeds the minimum power required.

The above conclusion is based on an ideal scenario with perfect impedance matching at the front end. In a real-world scenario, the effects of tag translation, rotation, and coupling, as well as the impact of environmental variation on the response rate must be considered and are discussed next. Our goal is to test the validity of the response rate as an index of signal intensity with experimental measurements. All experiments were performed by using the 915-MHz and 2.45-GHz RFID systems with passive tags.

A. Tag Translation

Figs. 4 and 5 show the relationship between the response rate and the distance for 915-MHz and 2.45-GHz systems, respectively, where the distance is measured between the centers of the tag and the reader's antenna.

We note from Figs. 4 and 5 that the behavior of the (mean) response rates for 915 MHz and 2.4 GHz are distinctly different.

1) For the 915-MHz system, the response rate saturates at both the low and high ends, suggesting two threshold values P_{th1} and P_{th2}, which determines the operating range for the response rate. When the energy level is higher than P_{th1}, the tag is in the saturation mode corresponding to $\alpha = 1$, while P_{th2} is the threshold for no response (i.e., $\alpha = 0$). Thus, the effective operating range

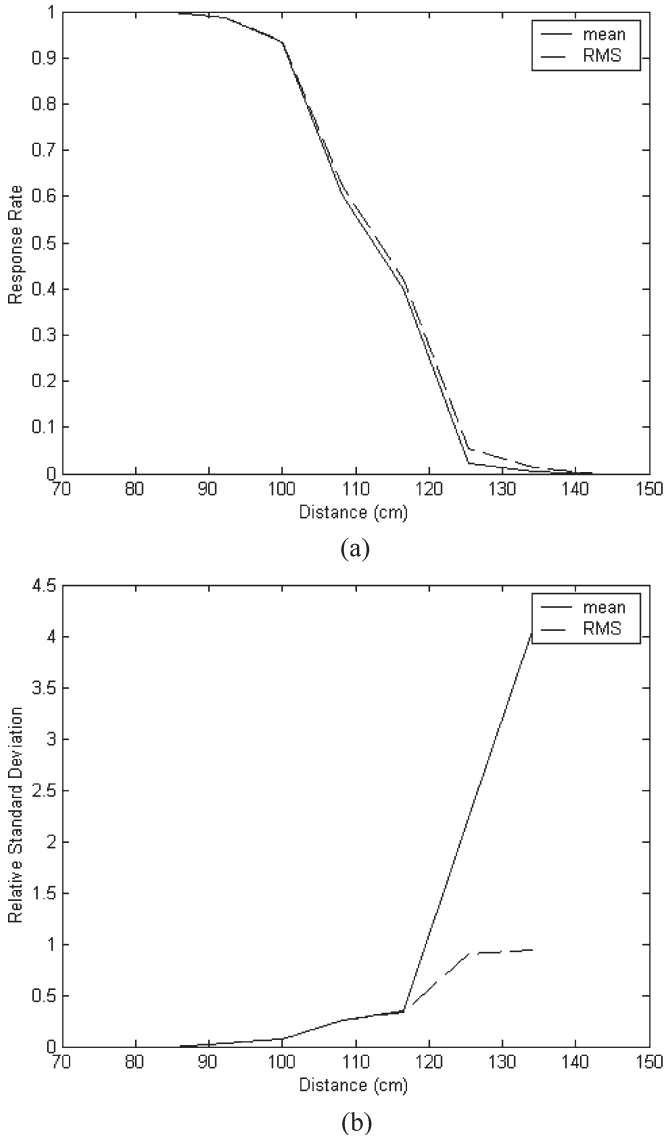

Fig. 4. Relationship between the response rate and translation (915-MHz system). (a) Reponse rate versus translation: 915 MHz. (b) Relative standard deviation versus translation: 915 MHz.

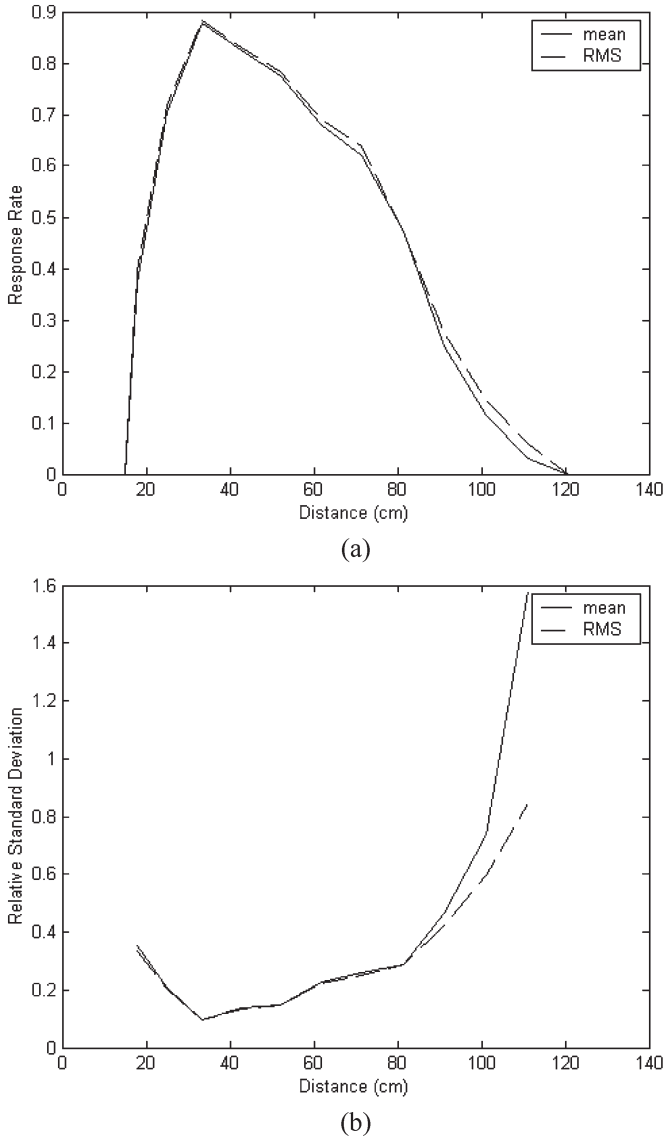

Fig. 5. Relationship between the response rate and tag translation (2.45-GHz system). (a) Response rate versus translation: 2.45 GHz. (b) Response standard deviation versus translation: 2.45 GHz.

if the spatial variation of energy is to be used to detect tag motion is given by

$$P_{\mathrm{th2}} \leq P_{\mathrm{r}} \leq P_{\mathrm{th1}} \tag{8}$$

where P_{th1} and P_{th2} are determined by the physical properties of the tag, the wavelength, as well as the antenna/RF front-end circuit used. The response rate for 2.45 GHz does not show saturation, i.e., P_{r} is always smaller than P_{th1} as shown in Fig. 5, implying a much-enhanced operating range.

2) The fields around an antenna are divided into two principal regions—the near field and the far field with boundary given by [6]

$$r = \frac{2L^2}{\lambda} \tag{9}$$

where L is the aperture of the antenna. The calculated r for 2.45 GHz (28 cm) conforms to the experimental result (33 cm) well. The near field is not observed in the 915-MHz system, since the minimum received power of the tag within the measurement range is higher than the upper threshold P_{th1}. We note that α_{mean} and α_{rms} are almost identical as expected and either can be used to represent the response rate. α_{mean} is used to represent the response rate in the following section, because it is easier to calculate.

3) In the reader antenna's far field, the sensitivity of the response rate with distance (i.e., the slope of the response rate) varies significantly from 0.25 to 0.04/cm in Fig. 5, but in general, is sufficient for motion detection. In the reader antenna's near field, this variation is much more limited.

4) In the far field, the relative standard deviation increases with distance and may also be used additionally to infer the distance.

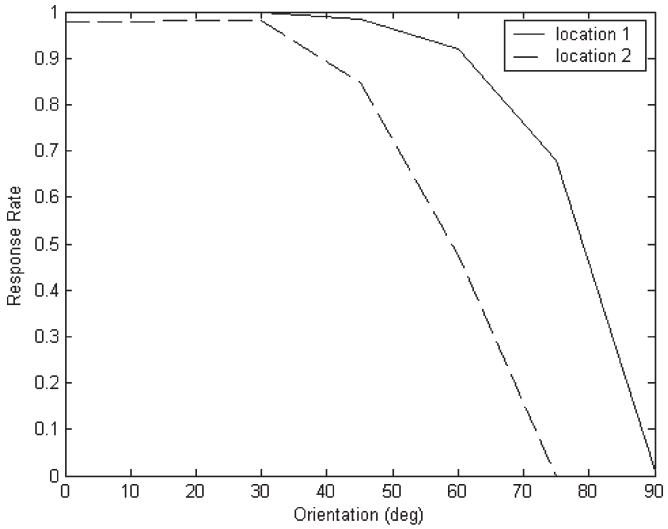

Fig. 6. Relationship between the response rate and the tag orientation.

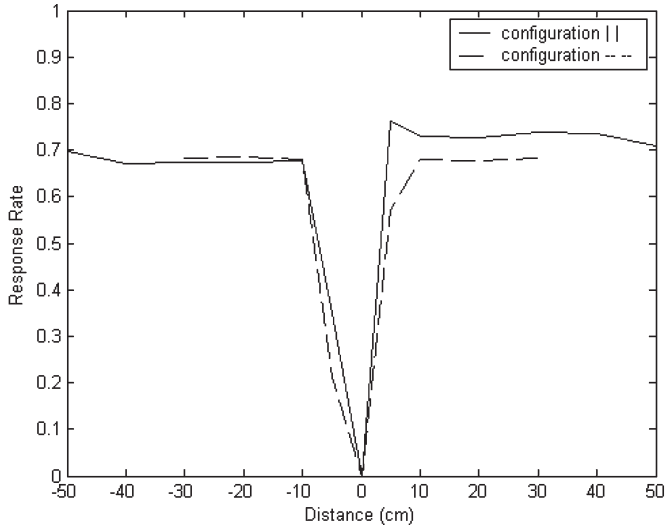

Fig. 7. Coupling effect on the response rate.

B. Rotation

Generally, the antennas of tags are $\lambda/2$ dipole antennas or folded $\lambda/2$ dipole antennas. For a matched tag antenna, its effective aperture $A_{\rm er}$ in (6) can be expressed as

$$A_{\rm er} = \frac{Z_0 h_{\rm e}^2 \cos^2\theta}{2R_{\rm r}} \tag{10}$$

where Z_0 is the intrinsic impedance of free space (377 Ω); θ is the angle between the tag orientation and the propagating wavefront from the reader; $h_{\rm e}$ is the effective height of the tag antenna, which is approximately 0.64 of the physical tag length [6].

Fig. 6 shows the variation of the response rate to tag orientation θ; the results do not conform well to the predicted $\cos^2\theta$ variation from (10). Further, the response rate is very sensitive to orientation change, which is a useful property for motion detection.

C. Coupling Between Tags

In the presence of other (interfering) tags around a desired tag in the reader's antenna field, the backscattered signal at the reader is altered due to the introduced mutual impedance. This can be expressed as

$$Z_{\rm R} = Z_{11} + Z_{12} = R_{11} - R_{12} + j(X_{11} - X_{12}) \tag{11}$$

where $Z_{\rm R}$ is the radiation impedance, Z_{11} (R_{11} and X_{11} are the resistive and reactive components of the self-impedance, respectively); and Z_{12} is the mutual impedance (R_{12} and X_{12} are the respective resistive and reactive components). The mutual-impedance computation is complex even when only two tags are in the field. For the special case of two $\lambda/2$ dipoles that are parallel, the net resistance of the dipole is given by [6]

$$R_{11} - R_{12} = 592.2\left(\frac{d}{\lambda}\right)^2 \tag{12}$$

where d is the distance measured between tag centers. The above equation is limited, only accurate within 5% when $d \le 0.1\lambda$. Fig. 7 shows the coupling effect when a tag is moved across a fixed distance. Two configurations were tested in experiments based on the motion of the interfering tag: the configuration "| |" indicates that the interfering tag is moved along the normal direction between the reader and desired tag while "- -" indicates tag motion perpendicular to the normal.

The following observations are pertinent.

1) When the two tags are close enough, neither will respond due to the mismatched radiation and load impedances. The voltage standing-wave ratio (VSWR) can be expressed as

$$\text{VSWR} = \frac{1+|\rho_v|}{1-|\rho_v|}, \quad \rho_v = \frac{Z_{\rm L} - Z_{\rm R}}{Z_{\rm L} + Z_{\rm R}} \tag{13}$$

where $Z_{\rm L}$ is the load impedance and ρ_v is the voltage-reflection coefficient. When $Z_{\rm R}$ deviates from $Z_{\rm L}$, a part of the energy is reflected. When the two tags are completely overlapped $(d = 0)$, (12) suggests that $R_{11} - R_{21} = 0$. Since it is known that $X_{12} = X_{11} = 43\ \Omega$ for two $\lambda/2$ dipoles [6], it follows that $Z_{\rm R} = 0$, and hence, VSWR $= \infty$. All the energy is thus reflected in this case, i.e., no energy is received. Thus, a "safe" zone is needed for the tags to be effective, i.e., only a limited number of tags must be allowed in the reader's antenna field. For example, the operating range of the reader's antenna used in experiments is about $0.6 \times 0.6 \times 1$ m^3, and the "safe zone" of a tag is about $0.2 \times 0.2 \times 0.2$ m^3; so the maximum number of tags allowed in this antenna field is about 45. The practical number may be much less than this due to environment factors and tag placement. Well-shaped tags could be used to alleviate the coupling effect.

2) Note that is possible for the response rate to increase when a second tag is nearby and is oriented parallel to the first (e.g., the spike at 5 cm in Fig. 8). This is caused

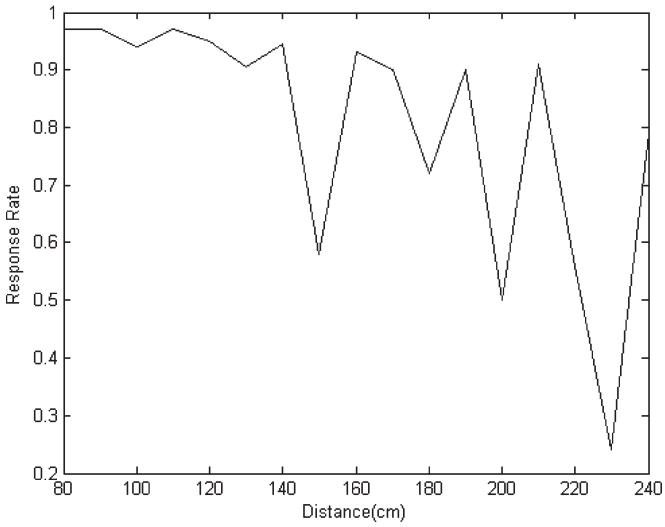

Fig. 8. Ceiling effect on the response rate.

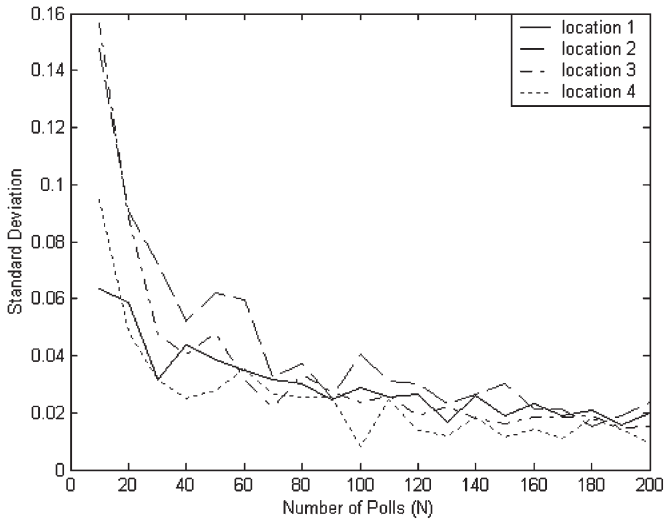

Fig. 9. Standard deviation as a function of N (number of polls per sample duration) with $N_{\mathrm{s}} = 10$.

by the fact that the fixed tag receives additional energy reflected by the second tag behind it.

D. Environment

The RF environment also has an important effect on the response rate, which is generally difficult to model. For example, tagged objects have a material permittivity ε, which could alter the radiation impedance of the tag's antennas significantly. The load impedance that is matched to the original (tag) radiation impedance is therefore mismatched when tags are attached to objects. This problem could be particularly serious when fluid or metallic objects are tagged. Other present readers may also have undesirable effects on the response rate. It was observed that a (second) remote interfering reader also negatively impacted (i.e., decreased) the response rate of the desired tag, although this tag is out of the formal range of second reader. Fig. 8 shows an example of the response rate caused by the superposition of a direct signal from the reader to tag along with the reflected wave components from the metal-framed ceiling, where the reader antenna is facing the ceiling and no other big objects are around. The response rate would remain fixed at one when there is no ceiling, which in Fig. 8 shows increased sensitivity to distance. Generally, the RF energy distribution fluctuates greatly in some indoor environments as compared to others. As a result, the utility of using the response rate for the detection of tag motion in such scenarios is greatly improved due to the presence of the multipath.

In summary, these experiments demonstrate the principled validity of using the response rate (which is an indirect metric of the received-signal-intensity level) in careful laboratory environments for detecting tag motion. Though a strict functional relationship between the response rate and the true received RF energy is difficult to predict, the sensitivity of the response rate to factors such as distance and tag orientation make this a useful approach. Note further the advantage of this technique in not requiring any hardware or communication-protocol modification. Nonetheless, the limited resolution of the response rate over the operating range of the system continues to be a major challenge.

IV. Tag-Movement-Detection Algorithms

We have argued that the change of the response rate can be used to detect the movement of tagged objects. To make this approach feasible in real time, two basic principles should be met for any proposed algorithm.

1) It must be able to detect the movement quickly.
2) It must be able to distinguish true tag movement from the false positives caused by the fluctuation of the response rate due to extraneous factors, e.g., short-term occlusion of the LoS connecting the reader and the desired tag or due to mutual coupling effects when a second tag is brought in the vicinity.

A. Selection of N and N_{s}

We intended to divide a continuous sampling set into N_{s} elements, where each element corresponds to N polls. A small N means a quick sampling action; therefore, a sudden change can be detected more quickly with a small N than a big N. However, it is unable to describe the accurate status when N is small, and a wrong decision could occur when several consecutive samples with big deviations are observed. Based on this point, a larger N is desired. Fig. 9 shows the relationship between the standard deviation σ and the number of polls (N). σ broadly decreases with increasing N, although there are local excursions. Therefore, a time-to-decision versus accuracy tradeoff is implied.

Another important parameter is the size of the sample set N_{s}. A suitable N_{s} value should be small enough for a quick decision and big enough to reach stable values of α_{mean} and σ. The minimum values of N_{s} required for the response rate to reach convergence varies as a function of location. Fig. 10 shows the relationship between the size of set N_{s} and the mean variation $(\alpha_{\mathrm{mean}}^{N_{\mathrm{s}}} - \alpha_{\mathrm{mean}})/\alpha_{\mathrm{mean}}$, where $\alpha_{\mathrm{mean}} = \lim_{N_{\mathrm{s}} \to \infty} \alpha_{\mathrm{mean}}^{N_{\mathrm{s}}}$. In the motion-detection algorithm, the selection of N_{s} should be adaptive to reach convergence with minimum delay.

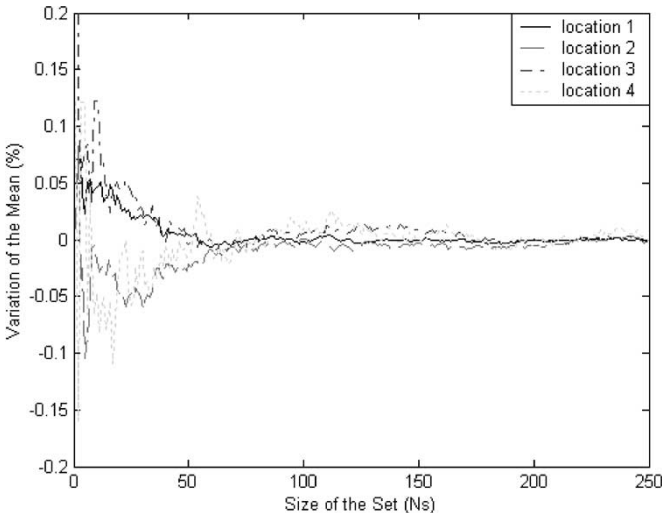

Fig. 10. Mean-value variation as a function of $N_{\rm s}(N = 10)$.

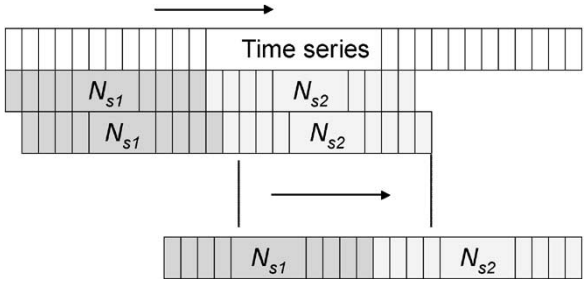

Fig. 11. Diagram of the sliding-window technique.

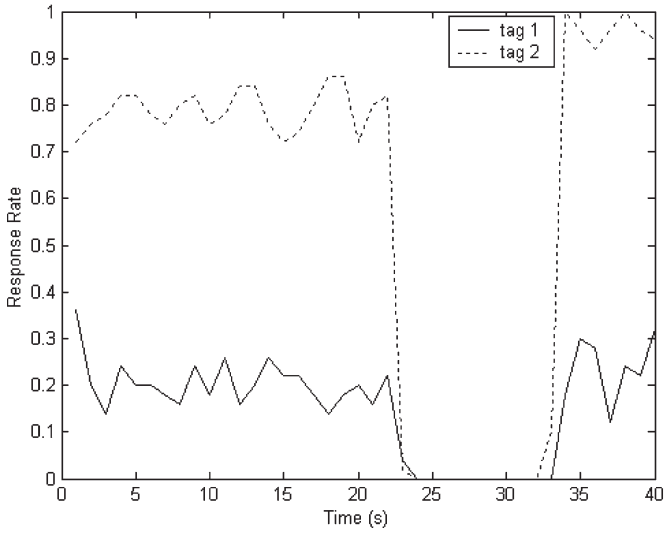

Fig. 12. Response rates of two coupled tags when a tag moved across the other tag.

B. Classes of Response-Rate Changes

Four classes of response-rate changes were identified and used in the detection schemes:

Type I: jump from/into saturation status: $\alpha_i = 1$ or a negligible standard deviation, i.e., $\sigma \approx 0$. σ or $\alpha_{\rm mean}$ are the pertinent statistics and smaller N_i, $N_{\rm s}$ are sufficient for reliable detection.

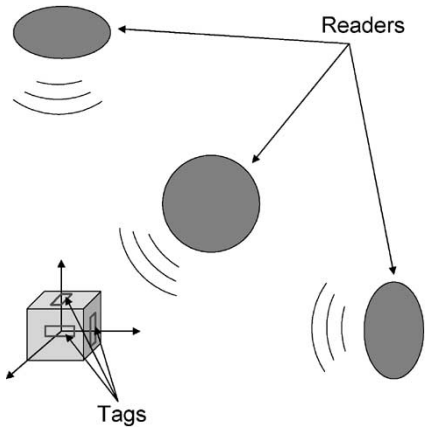

Fig. 13. Multitag configuration and the multireader configuration.

TABLE I
PEFORMANCE OF THE MULTIPLE-TAG/READER CONFIGURATION

Number of tags	Number of readers	1	2	3
1	blind spot	2 Dim.	1 Dim.	Φ
	block/reflect	1 Dim.	2 Dim.(1)	Φ
2	blind spot	1 Dim.	Φ/1 Dim.	Φ
	block/reflect	1 Dim.	2 Dim.(1)	Φ
3	blind spot	Φ	Φ	Φ
	block/reflect	1 Dim.	2 Dim.(1)	Φ

(1): certain human body postures could cause two dimensional blocking/reflection.

Type II: a jump from/into "out of range": $\alpha_{\rm mean} = 0$.

Type III: "large" change in the response rate: when a single new sample α_i is attained, it is compared with the mean value of the previous sample set via

$$\beta_i = \frac{|\alpha_i - \alpha_{\rm mean}|}{\sigma} \tag{14}$$

where β_i is the normalized bias and is used when $\sigma > 0$, i.e., the tag is neither in the saturation nor "out of range" status. We chose a threshold rule $\beta_i > 3$ to indicate that a tagged object was moved. Further, we approximate the distribution of β_i by the standard normal distribution, yielding a false alarm rate of less than 0.3%. This "big jump" detection statistic thus gives a faster decision as compared to the situation in Type IV below.

Type IV: mean value change. Here, the indication of tag motion is less definitive and more samples are needed for reliable decision. Thus, an entire new sample set is collected and the normalized magnitude difference between the new and old set means

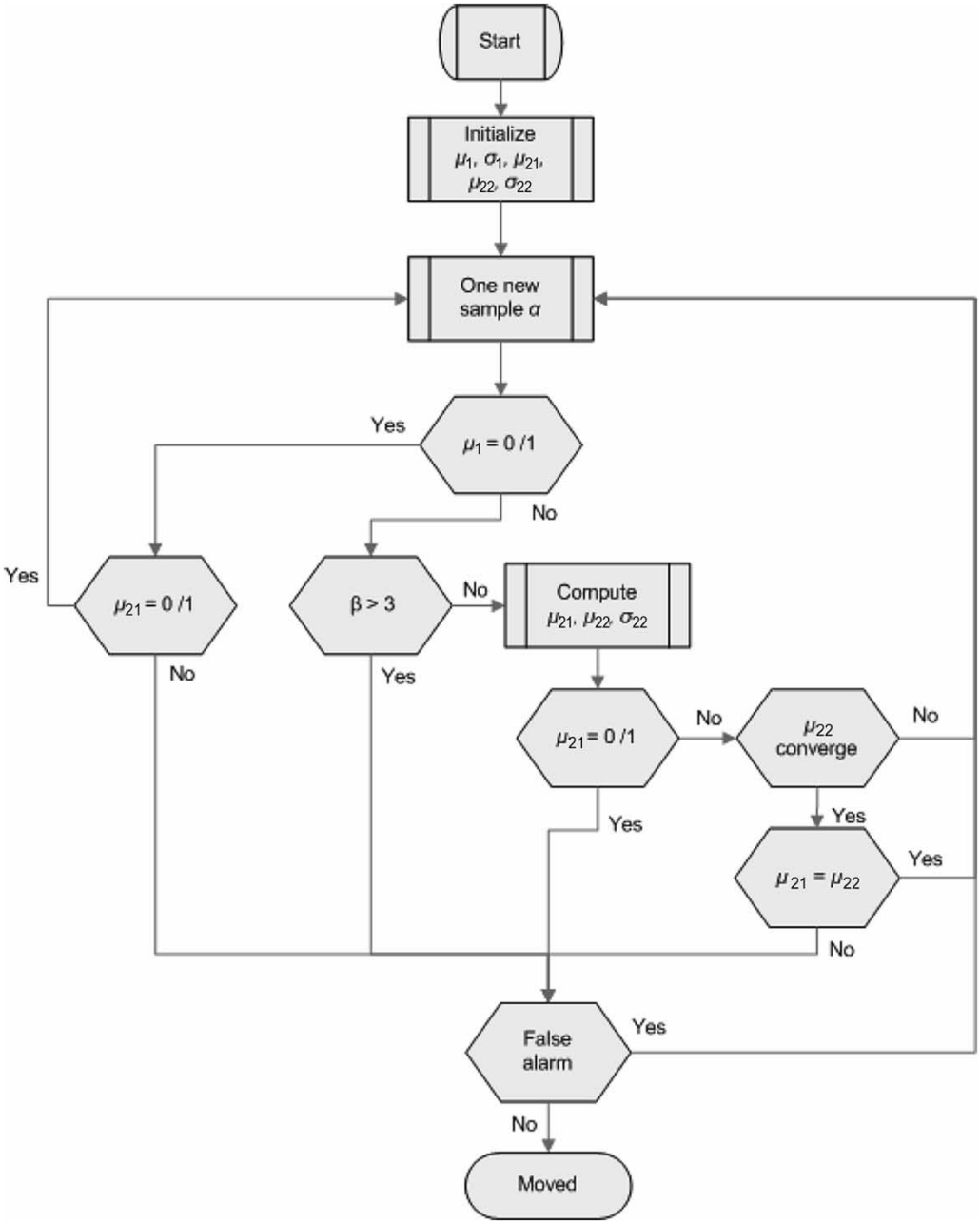

Fig. 14. Movement-detection algorithm.

is used. Obviously, this test has a slower response time in order to achieve desired accuracy.

In order to detect a Type I, II, or IV movement, a sliding window of response-rate samples is used in the algorithm, which greatly reduces computational burden and storage (Fig. 11). Two windows are used: window 1 follows the past state (reference), while window 2 tracks the current state. Both windows are back-to-back "first in, first out" queues such that the exiting sample from the window 2 goes into window 1. The size of window 2 is varied for detecting Type I/II and Type IV, respectively. The most important property of the sliding window is that there is always a time stamp such that the past (hypothesis of no motion) and the current (hypothesis of motion) states can be distinguished.

C. Exclusion of Coupling Effect

Although there is no way to differentiate the mutual coupling effect from real movement based only on the response rate of one tag, it is possible to derive the relationship of the time series from the two coupled tags by performing a correlation analysis; the false positives can be excluded when a significant correlation is observed. We assume that these two tags are attached on two different objects. The correlation coefficient is defined as [9]

$$r_{\mathrm{ce}} = \frac{\sum_{i=1}^{N_{\mathrm{s}}} (\alpha_{1i} - \alpha_{1\mathrm{mean}})(\alpha_{2i} - \alpha_{2\mathrm{mean}})}{(N_{\mathrm{s}} - 1)\sigma_1 \sigma_2} \tag{15}$$

where, r_{ce} is the correlation coefficient; α_{1i} and α_{2i} are the response-rate time series from two tags, respectively; σ_1 and

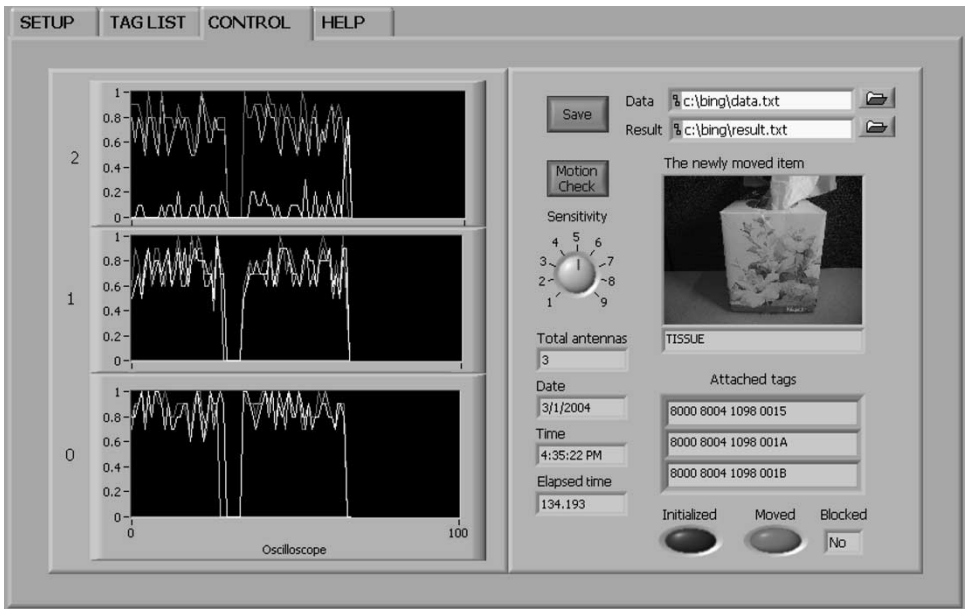

Fig. 15. Developed system for the movement detection of tagged objects.

σ_2 are the associated standard deviation. In order to prove the significance of $r_{\rm ce}$, Fisher's Z-transformation is used [9]

$$\frac{1}{2}\ln\left(\frac{1+\rho}{1-\rho}\right) = \frac{1}{2}\ln\left(\frac{1+r_{\rm ce}}{1-r_{\rm ce}}\right) \pm 1.96\sqrt{\frac{1}{N_{\rm s}-3}}. \quad (16)$$

When ρ_1 and ρ_2 are both large in amplitude with the same sign (ρ_1 and ρ_2 are solutions of (16) and $\rho_1 \leq \rho_2$), the result indicates a statistically significant relationship between the two series at the 95% confidence level. Fig. 12 shows an example of the coupling effect; the potential false detect is successfully excluded by this test (since $r_{\rm ce} = 0.88$, $\rho_1 = 0.78$, and $\rho_2 = 0.94$).

D. Multiple Tags/Readers

We have seen that our approach using the response rate for a single tag per object may only work within a short radial range or over a limited azimuth (angular) directions. The response rate can even include false movement due to reflection or blocking. We next propose using multitagged objects and/or multiple readers for enhanced system performance. Fig. 13 shows the configuration of the multitagged object and multiple readers. In order to fully explore the ability of multiple tags/readers, we need to place them along different independent axes due to orientation sensitivity, and readers should be circularly polarized antennas in order to overcome the orientation sensitivity of linearly polarized tags. The final active operating range would be the union of individual operating ranges; therefore, it results in greatly improved performance (Table I).

Interaction of other interfering objects (including the human body) and the desired tagged objects may be classified to a first order, as follows:

1) blocking whereby the interfering object obstructs the LoS between the reader and tag leading to a reduction of the power received by the tag;
2) an object in the vicinity that does not block the LoS, which nevertheless induces reflections that provide extra energy to the tag.

Thus, while blocking generally decreases the response rate, reflections may increase the response rate; nonetheless, both may result in false-motion indication. When there is only one tag/reader, there is no way to exclude such false positives. However, with multitags/readers, the occurrence of false positives could be reduced. We assume the tagged objects are much smaller than the human body, therefore it is impossible to have blocking and reflection at the same time. In other words, if we get both the increased and decreased response rates from the same tagged object, it is highly likely that the object has moved.

E. Motion-Detection System

Fig. 14 shows a flowchart of the movement-detection algorithms, where $\mu = \alpha_{\rm mean}$, μ_{21}, and μ_{22} are means for the two window 2's, respectively. Fig. 15 shows the graphical user interface (GUI) developed with LabView for the laboratory testing of our movement-detection system. Our early experiments show that the proposed method works well and reasonably quickly in detecting object motion in controlled environments. For example, when four tagged objects were placed in the reader antenna's field (Alien Technology Corporation's 915-MHz system), the system had the following performance: minimum (maximum) response time of 0.7 (7) s, respectively, and an average response time of around 2 s. For a total of 1353 experimental tests under different scenarios, the overall accuracy is 94% [10].

V. Conclusion

A novel approach to detect the movement of RFID-tagged objects was presented. The method does not require add-on hardware or communication-protocol modification and works

by analyzing changes in an easily derived approximation of signal-intensity level. System performance is greatly improved by introducing a multitag/reader configuration. The effect of tag movement on the response rate was categorized into four cases, which allow prompt and accurate detection. Experiments proved the validity of this cost-effective response-rate-based passive RFID system as a sensor network for movement detection.

REFERENCES

[1] V. Stanford, "Pervasive computing goes the last hundred feet with RFID systems," *IEEE Pervasive Comput.*, vol. 2, no. 2, pp. 9–14, Apr.–Jun. 2003.

[2] H. Stochman, "Communication by means of reflected power," *Proc. IRE*, vol. 36, pp. 1196–1204, Oct. 1948.

[3] J. Landt, "Shrouds of time—The history of RFID," in *RFID Connections*. Pittsburgh, PA: AIM Global, 2002, no. 2.

[4] M. Philipose, K. P. Fishkin, M. Perkowitz, D. Patterson, and D. Haehnel, "The probabilistic activity toolkit: Towards enabling activity—Aware computer interfaces," Intel Research Seattle, Seattle, WA, Tech. Memo. IRS-TR-03-013, Dec. 2003.

[5] K. Finkenzeller, *RFID Handbook: Fundamentals and Applications in Contactless Smart Cards and Identification*, 2nd ed. New York: Wiley, 2003.

[6] J. Kraus, *Antennas*, 2nd ed. New York: McGraw-Hill, 1988.

[7] Agilent Technologies Application Note 1089, *Designing Detector for RF/ID Tags*, Palo Alto, CA: Agilent Corporate.

[8] U. Karthaus and M. Fischer, "Fully integrated passive UHF RFID transponder IC with 16.7 μW minimum RF input power," *IEEE J. Solid-State Circuits*, vol. 38, no. 10, pp. 1602–1608, Oct. 2003.

[9] E. B. Mode, *Elements of Probability and Statistics*. Englewood Cliffs, NJ: Prentice-Hall, 1966.

[10] K. P. Fishkin, B. Jiang, M. Philipose, and S. Roy, "I sense a disturbance in the force: Long-range detection of interactions with RFID-tagged objects," in *Proc. 6th Int. Conf. Ubiquitous Computing*, Nottingham, U.K., 2004, vol. 3205, Lecture Notes in Computer Science, pp. 268–282.

Bing Jiang (S'01) received the B.S. degree from Tianjin University, China, in 1995, and the M.S.E.E. degree from the University of Washington, Seattle, in 2003. He is working toward the Ph.D. degree in the Department of Electrical Engineering, University of Washington.

He worked as an Intern at Intel Research, Seattle, from September 2003 to June 2004. He is interested in research on radio-frequency identification (RFID), sensors, and robotics.

Kenneth P. Fishkin received the B.S. degree in computer science and B.S. degree in mathematics from the University of Wisconsin, Madison, and the M.S. degree in computer science from the University of California, Berkeley.

He was previously a Senior Researcher at Intel Research, Seattle, when the work presented in this paper was performed. He is currently a Software Engineer at Google. He has published widely in the fields of radio-frequency identification (RFID), user interfaces, and computer graphics.

Sumit Roy (S'96–M'98) received the B.Tech. degree in electrical engineering from the Indian Institute of Technology, Kanpur, India, in 1983, and the M.S. and Ph.D. degrees in electrical engineering and the M.A. degree in statistics and applied probability from the University of California, Santa Barbara, in 1985, 1988, and 1988, respectively.

He is a Professor of electrical engineering at the University of Washington, Seattle, and a Visiting Faculty Consultant to Intel Research, Seattle. His areas of technical interest involve wireless communication systems. He is currently exploring the use of radio-frequency identification (RFID) and 802.11 wireless-local-area-network (WLAN) technologies within networked ubiquitous computing environments. He recently spent two years on academic leave at the Wireless Technology Development Group within Intel Labs, Hillsboro, OR, working on next-generation WLAN and personal-area-network (PAN) systems.

Prof. Roy is an active member of the IEEE Communications Society.

Matthai Philipose received the B.S. degree from Cornell University, Ithaca, NY, in 1994, and the M.S. degree from the University of Washington, Seattle, in 1996, both in computer science.

He is a Researcher at Intel Research, Seattle (IRS). His primary areas of interest are programming languages and probabilistic reasoning. He is currently working on human-activity inferencing at IRS.